IET Power Electronics

The Institution of Engineering and Technology WILEY

ORIGINAL RESEARCH

A quantitative harmonics analysis approach for sinusoidal pulse-width-modulation based Z-source inverters

Wenzheng Xu[1,2,3] | Chi Ho Chan[2,3] | Ka Wing Chan[2] | Siu Wing Or[2,3] |
Siu Lau Ho[2,3] | Ming Liu[2]

[1]School of Electrical Engineering, Beijing Jiaotong University, Beijing, China

[2]Department of Electrical Engineering, The Hong Kong Polytechnic University, Hung Hom, Kowloon, Hong Kong, China

[3]Hong Kong Branch of National Rail Transit Electrification and Automation Engineering Technology Research Center, Hong Kong, China

Correspondence
Prof. Siu Wing Or, CF627, Department of Electrical Engineering, The Hong Kong Polytechnic University, 11 Yuk Choi Road, Hung Hom, Kowloon, Hong Kong SAR, China.
Email: eeswor@polyu.edu.hk

Funding information
Research Grants Council of the HKSAR Government, Grant/Award Number: R5020-18; Innovation and Technology Commission of the HKSAR Government to the Hong Kong Branch of National Rail Transit Electrification and Automation Engineering Technology Research Center, Grant/Award Number: K-BBY1

Abstract

The shoot-through (ST) states are essential for the operation of sinusoidal pulse-width-modulation (SPWM) based Z-source inverters. However, the insertion of shoot-through state unavoidably leads to output harmonics which is greatly affected by its distribution, especially for bipolar modulation schemes. With quantitative analysis, this paper investigates the mathematical relationship between the output harmonics and shoot-through states for single-phase Z-source inverters. A modified double-Fourier-transformation-based calculation scheme is proposed to estimate the output harmonics with different shoot-through states insertion methods. Simulations and hardware experiments with a 200 W single-phase Z-source converter under two bipolar modulation control methods verified the accuracy of the proposed theory. The quantitative analysis would be helpful for the design of Z-source converter's control strategy and modulation scheme.

1 | INTRODUCTION

The integration of distributed renewable energy sources into the grid has long been a hot research topic, especially when microgrids are becoming more and more popular today. Power converters play a critical role in the energy transmission between distributed energy sources and the grid. With increasing distributed energy sources connected, it is essential to suppress the output harmonics of each power converter to guarantee the stability and quality of the grid. The output voltage and current harmonics of traditional pulse width modulation (PWM) full-bridge inverters have been well investigated in detail. For example, refs. [1] and [2] propose different space-vector control methods of three-phase inverters with the harmonics elimination capability. Meanwhile, dead time between the two switches

in one inverter bridge is essential to avoid short-circuit, leading to more harmonics. The effect of dead time on output harmonics was analysed with Fourier transformation [3], distortion shaping [4], and other compensation methods [5–10]. An analytical technique was proposed to calculate the output harmonics of an H-bridge inverter, considering the effect of dead time in [11–13]. Overall, the theory of calculating and suppressing output harmonics of a traditional PWM full-bridge inverter is relatively mature.

In recent decades, the Z-source converters have been proposed, which provide a single-stage voltage boosting inverter solution without the need for dead-time. Bi-directional single-phase and three-phase Z-source converters could be applied in vehicle-to-grid (V2G) as electric vehicle (EV)'s chargers. However, the harmonics of Z-source converters have long been a

problem influencing the output quality of currents injected into the grid. There is a compromise between the efficiency and the output harmonics in some instances. Moreover, although dead time does not exist in the control of Z-source inverters, ST states are inserted, which unavoidably produce output harmonics. The distribution of ST intervals in a switching period affects the system parameters, including output harmonics [14].

There is limited research investigating the output harmonics of Z-source inverters. Ref. [15] proposed a vector modulation scheme for current-fed quasi-Z-source inverters with different possible PWM switching sequences. By comparing the total harmonics distortion (THD) simulation results of each control sequence, the one with the smallest THD was adopted in the vector modulation. However, neither quantitative calculation nor theoretical analysis of the output harmonics and THD was included. The reasoning behind the selection of PWM sequence leading to the smallest harmonics is desired. Similarly, ref. [16] proposed a novel phase-shifted control method with harmonics elimination capability for Z-source inverters with three possible cases. While Case 3 in [16] with $\beta_{sh} > \alpha$ leads to the lowest output THD according to the computation results and experiments, there is no mathematical theory to further support it. Ref. [17] introduced the primary ST states insertion schemes and compared their corresponding common-mode voltages and output harmonics for three-phase quasi-Z-source inverters. Still, there is no analysis or investigation of the harmonic results. In short, the output harmonics of Z-source inverters deserve further research of in-depth quantitative analysis, especially its relationship with the insertion of ST states.

Harmonics suppression or compensation methods of traditional SPWM inverters in literature [18–20] are studied and referred in this paper to analyse Z-source inverters because of the similarity between the effects of dead time and ST states on the inverter's output harmonics. A circulating current model was built [21] to analyse the influence of dead time with different PWM schemes for three-phase inverters. Moreover, a series of harmonics compensation or suppression control approaches for conventional inverters [22–27] were proposed for the motor drive or microgrid applications. Though the proposed quantitative analysis of ST states and output harmonics is inspired by the above literature for conventional PWM inverters, the intrinsic differences between traditional inverters and Z-source inverters have made the analysis complicated and challenging.

This paper proposes a new quantitative analysis approach for single-phase Z-source inverters based on the foundation in [3] by double Fourier transformation. A comparison of the semi-symmetric "$a+b$" control method and the asymmetric "$a+b$" method based on bipolar modulation is conducted to verify the proposed approach and explain the reason for their difference in output harmonics. The proposed approach allows researchers to evaluate, estimate and calculate the output harmonics of Z-source inverters with different bipolar ST states insertion schemes more conveniently.
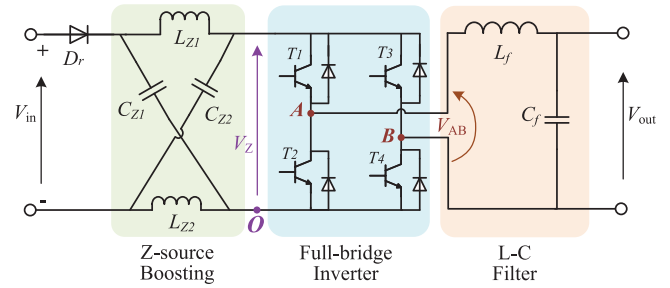

FIGURE 1 Topology of a single-phase Z-source inverter

The organization of this paper is as follows: Section 1 introduces the literature review and explains the importance of this research. Section 2 analyses the ST states and their effects on Z-source inverters with SPWM control strategy. Section 3 introduces the proposed quantitative analysis method with double Fourier transformation in detail. Section 4 presents the simulation results by comparing two control methods with different ST states insertion schemes. Experimental results with discussions are presented in Section 5. Lastly, a conclusion is given in Section 6.

2 | OPERATION ANALYSIS WITH ST STATES

2.1 | Key waveforms of single-phase Z-source inverters

Figure 1 presents a common un-isolated single-phase Z-source inverter. There are two steady-state periods in the operation of this Z-source inverter, namely shoot-through state (ST state) and non-shoot-through state (non-ST state). In ST states, the voltage across the Z-source topology $V_Z = 0$ because the bridge is short-circuited. Similarly, the diode D_r is blocked since V_Z is more significant than the input voltage V_{in}. In non-ST states, the diode D_r is forward biased.

The duty cycle D of the ST state is greater than 0 and smaller than 1, so the average voltage V_Z must be higher than V_{in}. If ST states are prolonged, V_{out} and voltage gain will increase. Therefore, the single-phase Z-source inverter is capable of inverting with boosting. This single-stage voltage boosting inversion makes full use of ST states. The single-phase Z-source inverter eliminates the need for dead time between the two switches in one bridge, enhancing the system reliability.

Among the five types of control methods of a single-phase Z-source inverter, that is, one-cycle PWM control, modified reference PWM, hysteresis current control, non-linear sinusoidal PWM and low-frequency harmonics elimination PWM, shoot-through by overlapping of active states would lead to minimum switching loss and higher efficiency [9, 26]. The effects of ST states on voltage waveforms V_{AO}, V_{BO} and V_Z are illustrated in Figure 2. While both ST state and dead time would lead to harmonics, only the ST state in
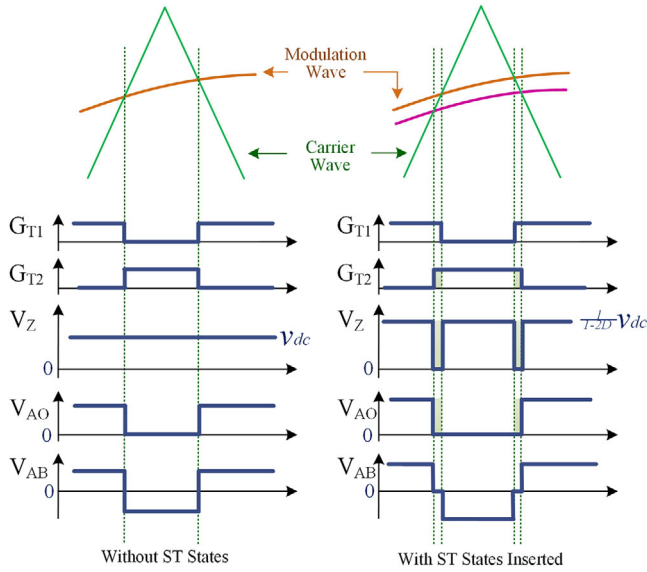
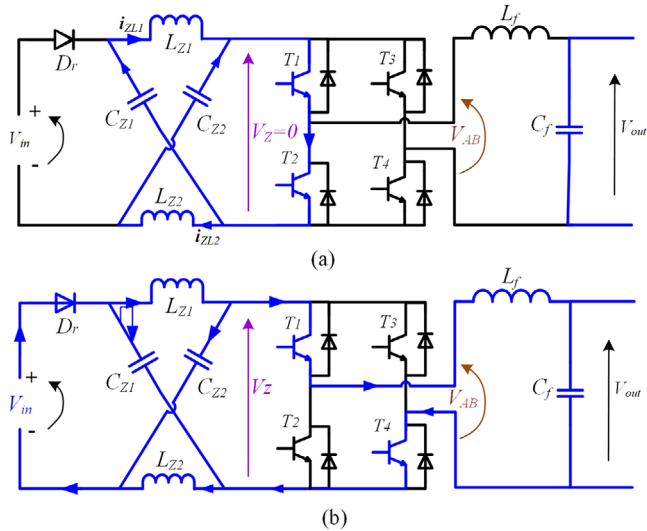**FIGURE 2** Voltage waveforms with ST states effects

FIGURE 3 Steady-sates operation modes of Z-source inverters. (a) ST state (b) non-ST state: T_1, T_4 turned on as an example

Z-source inverters could lead to the voltage boosting of V_z. As shown in Figure 2, the voltage V_{AB} and switching states are strongly influenced by ST states during one switching cycle. The time instant of switching angles varies due to the presence of ST states, and the harmonic characteristics would vary accordingly.

The operation of the Z-source inverter is classified into two periods in steady states: ST state period and non-ST state period [27]. The total time length of the ST state in one cycle is defined as Ts, then the duty cycle D of the ST state is equal to T_s/T. As mentioned before, the full-bridge is short-circuited in the ST state, so the voltage across the Z-source topology V_Z is zero. As illustrated in Figure 3a, V_Z is more significant than V_{in}, so the diode D_r is reversely biased. In non-ST states, the diode D_r

is forward biased as shown in Figure 3b.

$$\frac{d}{dt}\begin{bmatrix} i_{L1}(t) \\ i_{L2}(t) \\ v_{C1}(t) \\ v_{C2}(t) \end{bmatrix} = \begin{bmatrix} 0 & 0 & \frac{2D-1}{L_Z} & 0 \\ 0 & 0 & 0 & \frac{2D-1}{L_Z} \\ \frac{-D}{C_Z} & \frac{1-D}{C_Z} & 0 & 0 \\ \frac{1-D}{C_Z} & \frac{-D}{C_Z} & 0 & 0 \end{bmatrix}$$

$$\cdot \begin{bmatrix} i_{L1}(t) \\ i_{L2}(t) \\ v_{C1}(t) \\ v_{C2}(t) \end{bmatrix} + \begin{bmatrix} \frac{1-D}{L_Z} \\ \frac{1-D}{L_Z} \\ 0 \\ 0 \end{bmatrix} \cdot V_{in} + \begin{bmatrix} 0 \\ 0 \\ \frac{D-1}{C_Z} \\ \frac{D-1}{C_Z} \end{bmatrix} \cdot i_Z \quad (1)$$

The state-space equations are presented in (1). To obtain the steady-state parameters, Equation (1) should be zero.
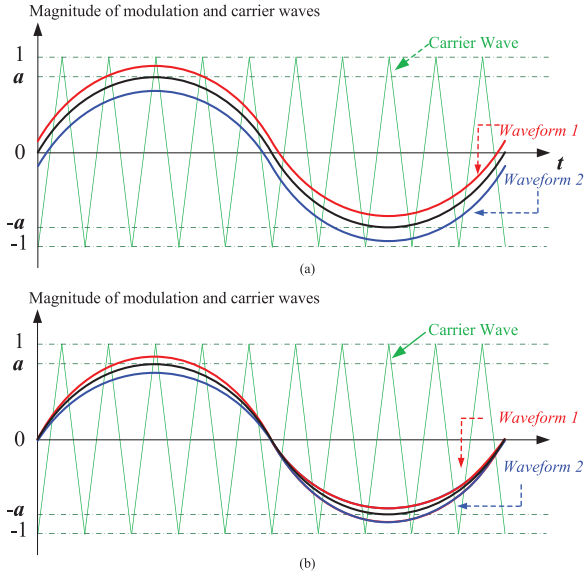
2.2 | Different ST states insertion pattern

ST states are widely spread over the whole operation cycle with the proposed control methods in [9]. In this way, the Z-source topology could play the role of the front-end boost converter for a DC-AC converter. The voltage across the inverter bridge V_{AB} shifts between $+V_Z$, $-V_Z$ and 0, as shown in Figure 1. This paper would introduce two ST states methods, leading to evenly and unevenly distributed ST states.

In Figure 4, the green sawtooth curve represents the carrier wave with magnitude of 1, and frequency of 10 kHz in this paper. The magnitude of the black modulation wave is a in the range of $0 < a < 1$. In Figure 4a, two modulation waveforms marked red and blue are generated by adding and subsiding a positive constant to produce overlapping active states. The modified red modulation wave generates switching signals of T2 and T3, while the red curve generates switching signals of T1 and T4. If b is the positive constant, the magnitude of the modified blue modulation wave will vary from $-a-b$ to $a-b$. Equation (2) shows the equations of the three modulation waves.

$$m_{black} = a \cdot \sin \omega t$$
$$m_{red} = a \cdot \sin \omega t + b \quad (2)$$
$$m_{blue} = a \cdot \sin \omega t - b$$

Figure 4b shows the modified modulation waves of the second scheme defined by (3) with the magnitudes of waveform 1

FIGURE 4   Modulation waveforms with different ST states insertion. (a) Evenly distributed ST states. (b) Unevenly distributed ST states

TABLE 1   Range of modified modulation waves

|		Minimum magnitude	Maximum magnitude	Magnitude when $t = 0$
Evenly distributed ST states	Waveform 1	$-a+b$	$a+b$	b
	Waveform 2	$-a-b$	$a-b$	$-b$
Unevenly distributed ST states	Waveform 1	$-a+b$	$a+b$	0
	Waveform 2	$-a-b$	$a-b$	0

m_{red} always larger than or equal to that of waveform 2 m_{blue} to produce overlapping of those two waves so that unevenly distributed ST states could be inserted.

$$
\begin{cases}
m_{black} = a \cdot \sin \omega t \\
m_{red} = (a + b) \cdot \sin \omega t, 0 < \omega t < \pi, \\
\qquad (a - b) \cdot \sin \omega t, \pi < \omega t < 2\pi \\
m_{blue} = (a - b) \cdot \sin \omega t, 0 < \omega t < \pi, \\
\qquad (a + b) \cdot \sin \omega t, \pi < \omega t < 2\pi
\end{cases}
\tag{3}
$$

Table 1 summarizes the ranges of the modified modulation waves from the two proposed bipolar modulation schemes that effectively reduce the common-mode voltage. Their differences in distribution characteristics and insertion patterns of ST states are shown in Figure 5.
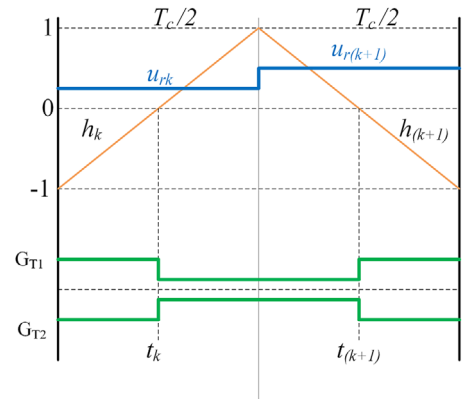
3 | HARMONICS QUANTITATIVE ANALYSIS

This section investigates the relationship between the output voltage harmonics and ST states insertion pattern for bipolar-
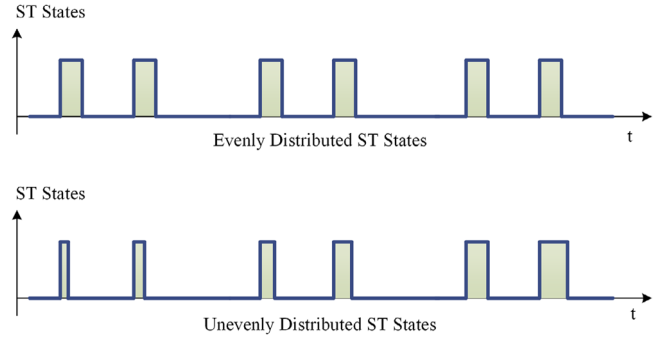
FIGURE 5   ST states insertion pattern

TABLE 2   Definition of symbols

Symbol	Definition
ω_c	Angular frequency (triangular carrier)
θ_c	Phase shift angle (triangular carrier)
ω_m	Angular frequency (fundamental)
θ_m	Phase offset angle (fundamental)
m	Baseband index variable
c	Carrier index variable
a	Modulation ratio

FIGURE 6   Principle of switching angle generation

modulation based control methods of Z-source inverters by quantitative analysis.

Based on the literature review, the double Fourier series method has more advantages. In SPWM harmonics analysis, different initial phase angles will not affect the result with a modified double Fourier series method, as described below. The harmonic voltage models with and without the influence of ST states are created. For convenience, terms listed in Table 2 are defined.

Firstly, the traditional double Fourier series equation is [28]:

$$f(t) = \frac{A_{00}}{2}$$

$$+ \sum_{m=1}^{\infty} [A_{0m} \cos(m \cdot (\omega_m t + \theta_m)) + B_{0m} \sin(m \cdot (\omega_m t + \theta_m))]$$

$$+ \sum_{c=1}^{\infty} [A_{c0} \cos(c \cdot (\omega_c t + \theta_c)) + B_{c0} \sin(c \cdot (\omega_c t + \theta_c))]$$

$$+ \sum_{c=1}^{\infty} \cdot \sum_{\substack{m=-\infty \\ m \neq 0}}^{\infty} A_{cm} \cos[c \cdot (\omega_c t + \theta_c) + m \cdot (\omega_m t + \theta_m)]$$

$$+ \sum_{c=1}^{\infty} \cdot \sum_{\substack{m=-\infty \\ m \neq 0}}^{\infty} B_{cm} \sin[c \cdot (\omega_c t + \theta_c) + m \cdot (\omega_m t + \theta_m)]$$

$$\tag{4}$$

$$A_{cm} = \frac{1}{2\pi^2} \int_{-\pi}^{\pi} \int_{-\pi}^{\pi} f(\omega_c t + \theta_c, \omega_m t + \theta_m) \cdot \cos[c(\omega_c t + \theta_c)$$

$$+ m(\omega_m t + \theta_m)] d(\omega_c t + \theta_c) d(\omega_m t + \theta_m)$$

$$B_{cm} = \frac{1}{2\pi^2} \int_{-\pi}^{\pi} \int_{-\pi}^{\pi} f(\omega_c t + \theta_c, \omega_m t + \theta_m) \cdot \sin[c(\omega_c t + \theta_c)$$

$$+ m(\omega_m t + \theta_m)] d(\omega_c t + \theta_c) d(\omega_m t + \theta_m)$$

$$\tag{5}$$

In (4), ω_m and θ_m represent the frequency and phase angle of low-frequency modulation wave, while ω_c and θ_c represent the frequency and phase angle of the high-frequency carrier wave. If they express periodic variables $x(t)$ and $y(t)$, the waveform is presented as function $f(x,y)$, that is, $f(t)$ showing the relationship between its value and time. A_{cm} and B_{cm} represent corresponding coefficients in the Fourier transformation. Among them, $A_{00}/2$ represents the DC component of the waveform. The second/third line of (4) represents the modulation wave and carrier wave baseband harmonics, the fourth/fifth line of (4) represents the sideband harmonics around the carrier harmonics [29]. The subscripts c and m represent the index number of the carrier wave and modulation wave, which are multiples of the two waveform frequencies.

Figure 6 shows how switching angle is generated during the modulation of switching signals. Transforming the coefficients A_{cm} and B_{cm} into the polar form, the following equation could be obtained:

$$H_{cm} = A_{cm} + jB_{cm}$$

$$= \frac{1}{2\pi^2} \int_{-\pi}^{\pi} \int_{-\pi}^{\pi} f(x,y)e^{j(cx+my)} dxdy \tag{6}$$

where $x = \omega_c t, y = \omega_m t$. The harmonic amplitude H_{cm} meets:

$$H_{cm}^2 = A_{cm}^2 + B_{cm}^2 \tag{7}$$

Concerning asymmetric cases, two sampling points are generated in each period of the carrier wave. The modulation wave

angel y_k can be expressed as

$$y_k = \frac{\omega_m}{\omega_c}(k-1)\pi \tag{8}$$

where k is a string ranges from 1 to $2N$, and

$$y_k = y - \frac{\omega_m}{\omega_c}[x - (k-1)\pi] \tag{9}$$

where a is the modulation index as described in last section.

A function $r(\lambda)$ is defined with λ representing whether it corresponds with the rising edge or falling edge. For the rising edge, $r(\lambda)$ is equal to -1; for the falling edge, $r(\lambda)$ is equal to 1. Symbol x_k is switching angle corresponds to the carrier wave, which can be expressed as:

$$x_k = \frac{\pi}{2} + (k-1)\pi + r(x_k)\Delta x_k \tag{10}$$

$$x_k = \frac{\pi}{2} a \sin y_k \tag{11}$$

The result in (11) for switching angle is available at any initial angle. The harmonic coefficient could be rewritten as:

$$H_{cm} = \frac{V_{in}r(x_k)}{4\pi^2} \left(\begin{array}{l} \int_0^{2\pi} \int_0^{xk} e^{j(cx+my)} dxdy - \int_0^{2\pi} \int_{xk}^{x(k+1)} e^{j(cx+my)} dxdy \\ + \int_0^{2\pi} \int_{x(k+1)}^{2\pi} e^{j(cx+my)} dxdy \end{array} \right) \tag{12}$$

Because of the symmetry feature, (12) can be simplified as:

$$H_{cm} = \sum_{k=1}^{N} r(x_k) e^{jks\pi} e^{r(x_k)js\frac{\pi}{2}a \sin y_k}$$

$$\cdot \frac{-V_{in}\omega_m}{2js\pi\omega_c}[(-1)^{(Nc+m)} - 1]e^{-js\frac{\pi}{2}} \tag{13}$$

$$s = m + c(\omega_m/\omega_c) = m + c/N \tag{14}$$

As shown above, the ST states effects lead to the time delay T_d of u_a when the phase current i_a is positive. In the same way, the time delay T_s occurs when $i_a < 0$. The effect of ST states on switching angle x_k based on the angle of the carrier is illustrated in Figure 7, where the symbol $\Delta\theta$ represents the time delay according to the carrier wave angel. Figure 7a shows an overview of the effect of ST states in one modulation cycle, and Figure 7b shows a specific view during one switching cycle.

The time delay could be expressed as:

$$\Delta\theta = \omega_c T_d \tag{15}$$
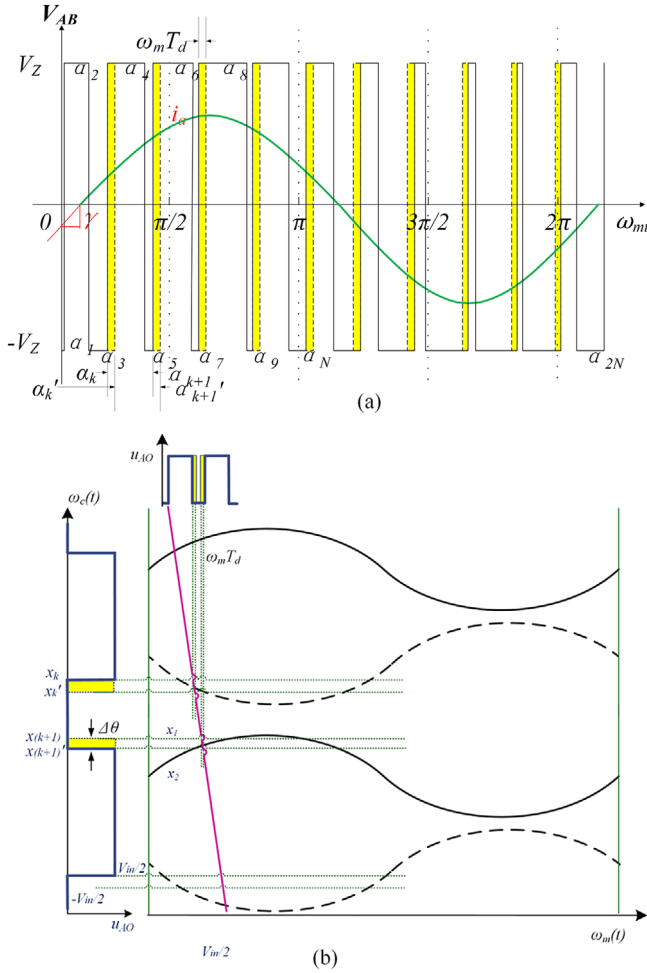
FIGURE 7 ST states analysis with switching angle a_k and x_k. (a) Overview during one modulation period, (b) specific view during one switching cycle

The additional harmonic component produced by ST states could be expressed as:

$$\Delta H_{cm} = \frac{V_{in}}{4\pi^2} \int_0^{2\pi} \int_{xk}^{xk'} e^{j(cx+my)} dx dy [r(x_k) - s(i)] \quad (16)$$

where $s(i)$ corresponds to the current direction. When the current direction is positive, $s(i)$ is defined as 1; otherwise, $s(i)$ is defined as -1. The switching angles with ST states are:

$$x_k' = x_k + \frac{1 - s(i)r(x_k)}{2}\Delta\theta \quad (17)$$

The additional harmonic component of the ST states H_{cm} could be obtained:

$$\Delta H_{cm} = \frac{V_{in}}{2js\pi} \frac{\omega_m}{\omega_c} \sum_{k=1}^{2N} \left[e^{js\frac{1-s(i)r(x_k)}{2}\Delta\theta} - 1 \right] \cdot r(x_k) e^{jsxk} \quad (18)$$

TABLE 3 The calculation times of each item

|	$x+y$	x/y	$\sin(x)$
Without ST states	$3N+2$	$6N+10$	N
With ST states	$17N-3$	$24N+16$	$2N$

According to (13), the harmonics do not exist as $N_c + m$ is the harmonic order, the term $N_c + m$ is an odd number. The total harmonics of the bridge voltage with ST states inserted can be obtained by combining (13) and (18). The double Fourier series method is adopted to calculate and investigate the effects of corresponding modulation wave and carrier wave angles on the output harmonics. Since both the modulation wave and carrier wave angles are considered, the harmonics distribution pattern could be derived by double Fourier series method with the above equations. Meanwhile, since the ratio of modulation wave frequency over carrier wave frequency is also considered in (14), the effect of the carrier wave ratio on output THD could also be calculated by the double Fourier series method. Regarding the computation burden, Table 3 shows the calculation times of each item, including adding/subsiding, multiplication/division, exponents, and sinusoidal calculation.

The proposed quantitative harmonic analysis approach is suitable for bipolar-modulation based control methods of Z-source inverters only. For unipolar-modulation, Equations (10)–(18) and Figure 7 should be revised accordingly.

4 | SIMULATION VERIFICATION

Simulations in MATLAB Simulink were conducted to verify the proposed harmonics quantitative analysis method by presenting and comparing the output harmonics of different ST states insertion patterns. Figure 8 shows the two modulation waves for generating evenly-distributed ST states and generating unevenly-distributed ST states, respectively.

The topology in the simulation is exactly the same as Figure 1. The rated input DC voltage is 100 V, and the rated output peak voltage is 200 V. The simulation is conducted using ode23tb (stiff/TR-BDF2) solver with variable step and a sampling time of 1 μs. As the output harmonics are significantly affected by the LC filter, only harmonics of the bridge voltage V_{AB} and dc-link Z-source voltage V_Z are analysed. Figure 9 shows the V_Z waveforms of the evenly-distributed ST states method. As there is little difference with the waveforms of the unevenly-distributed ST states method, they are not presented here. During ST states, voltage V_Z is clamped to zero. In non-ST states, voltage V_Z is boosted higher than input DC voltage. Ideally, the dc-link voltage V_Z of this inverter is a high-frequency rectangular wave, which alters between $V_{in}/(1-2D)$ and 0, as shown in Figure 2. However, the two control methods are based on bipolar modulation schemes. Since the switching frequency in simulation and experiment is 10 kHz, which is 100 μs for a period, the ST states occur at most four times within 100 μs considering there are two bridges. When the modulation wave magnitude is close to 1 or
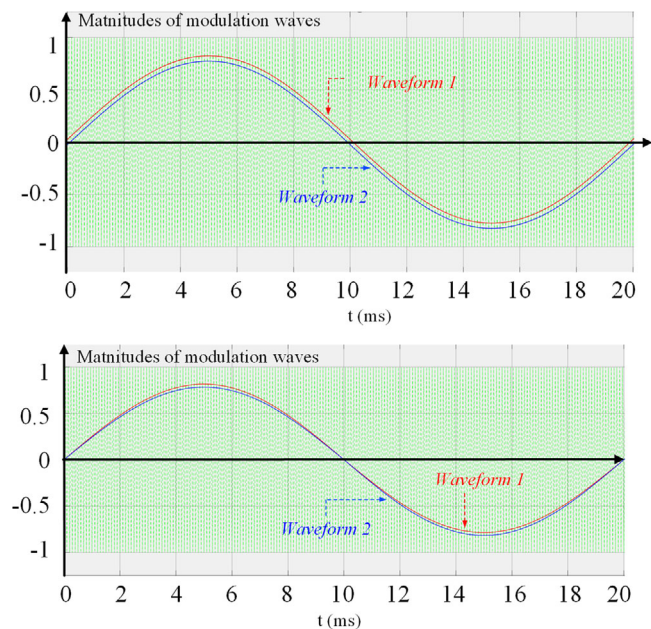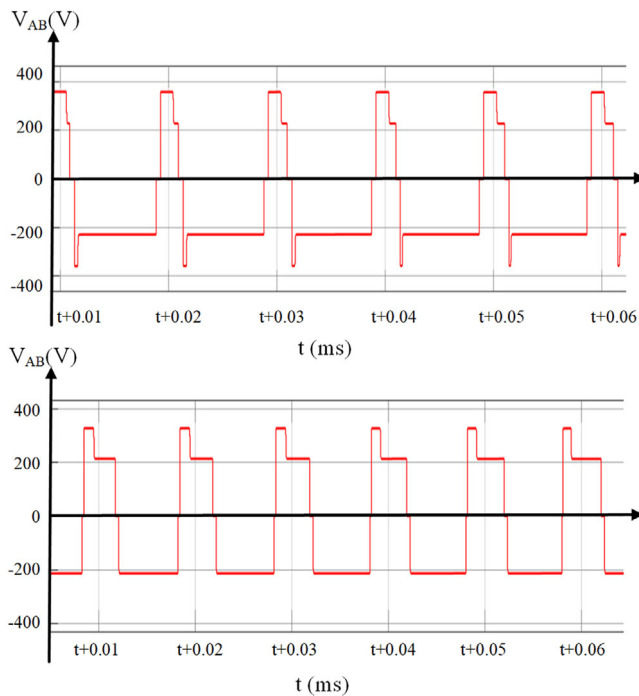
FIGURE 8 Simulation results of modulation waveforms of two methods. (a) Evenly-distributed ST states method. (b) Unevenly-distributed ST states method
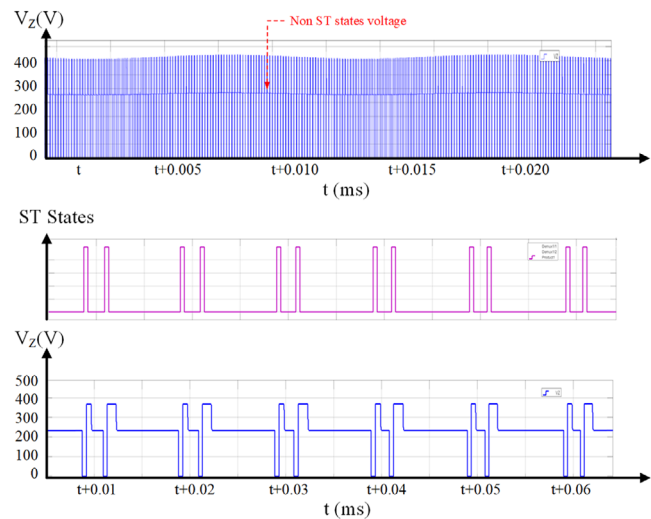
FIGURE 9 Simulation waveforms of dc-link voltage V_Z. (a) Overview over one modulation cycle. (b) Zoom view over six switching cycles

FIGURE 10 Simulation waveforms of bridge voltage V_{AB}. (a) Evenly-distributed ST states method. (b) Unevenly-distributed ST states method

TABLE 4 Comparison of calculated harmonics with simulations with 100 V input voltage

Harmonic order	Evenly-distributed ST states		Unevenly-distributed ST states	
	Calculation	Simulation	Calculation	Simulation
200	91.6%	92.9%	88.0%	88.8%
400	43.6%	43.6%	40.4%	41.5%
600	34.9%	31.1%	26.1%	28.9%
800	17.5%	16.2%	20.2%	17.8%

−1, the time slot between the two ST states will be very narrow. For bipolar modulation, the phase transition is interrupted by the ST states, and in such cases voltage V_Z could not vary to its steady magnitude within such a short time. There are spikes as observed in Figure 9a whose magnitude reaches 500 V, while the non-ST state voltage of V_Z is around 240 V as marked by the red arrow. Figure 10 presents the waveforms of bridge voltage V_{AB} for both evenly-distributed ST states method and evenly-distributed ST states method, respectively. The voltage across the inverter bridge V_{AB} shifts between $+V_Z$, $-V_Z$ and 0. The peak magnitudes of V_{AB} are also affected by the voltage spikes of V_Z.
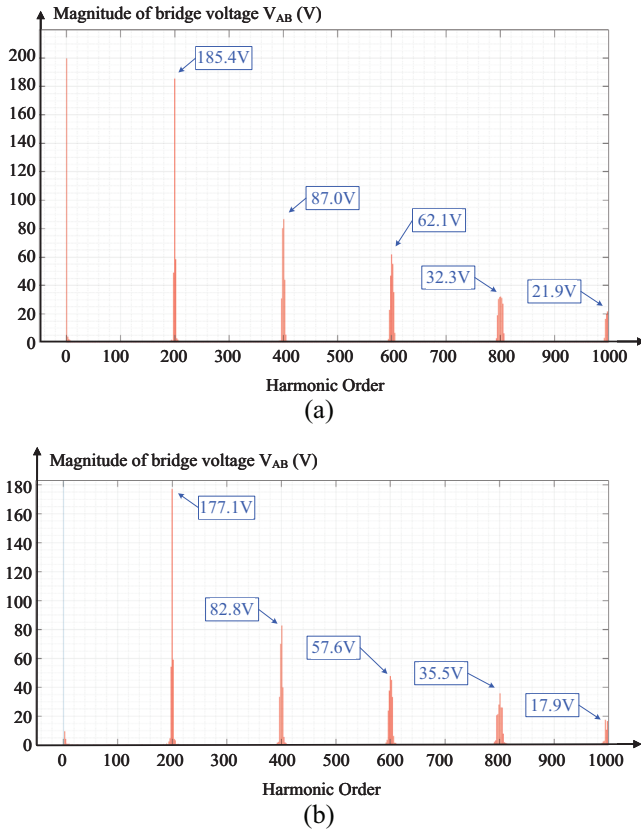
In particular, FFT analysis at integral times of switching frequency for 1–1000 harmonic order is presented in Figure 11. Since the switching frequency is 10 kHz, 200 times higher than the modulation wave's frequency (50 Hz), the harmonic at times of 200 order is significantly high. In comparison, it is evident that the harmonics of evenly-distributed ST states are higher than that of unevenly-distributed ST states. This result also matches the calculation results by Equations (5)–(16).

Table 4 listed the calculated output voltage harmonics and corresponding simulation results at 200, 400, 600 and 800 harmonic orders. It proves the correctness and accuracy of the proposed calculation method. Moreover, it is verified that the output harmonics with the evenly-distributed ST states method are greater than those with the unevenly-distributed ST states. It is worth noting that since this paper investigates the harmonics quantitatively, the harmonic magnitude of inverter bridge V_{AB}
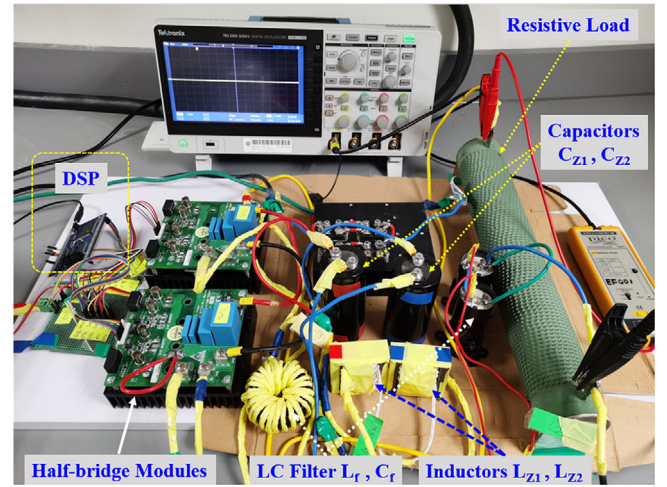
FIGURE 11   FFT analysis at integral times of switching frequency for from 1–1000 harmonic order. (a) Evenly-distributed ST states method. (b) Unevenly-distributed ST states method

FIGURE 12   Hardware setup

TABLE 6   Models and attributes of devices

Device	Model	Attributes
Half-bridge modules	Wolfspeed KIT8020 CRD8FF1217P-1	Maximum V_{DS} 1200 V Continuous I_D 10 A
Anti-parallel diode	C4D20120D	Drain current: 20 A
Input diode D_r	IXYS DSEI2 × 31-10b	Reverse voltage 1000 V Forward current 60 A
Z-source capacitors C_Z	Aluminium electrolytic capacitor	2200 μF, 450 V_{dc}
Output filter capacitor C_f	Aluminium electrolytic capacitor	80 μF, 260 V_{ac}

is presented and compared to avoid the influence of the LC filter.

In short, Figures 6 and 7 illustrate the correspondence between the symbols in Fourier Equations (4)–(18) and modulation/carrier wave magnitudes and frequency. The calculation results of two insertion methods by adopting these equations are presented in Table 4. The significant difference between the two insertion methods is the distribution of ST states, as shown in Figure 5. Its reflection on the Fourier Equations (13)–(18) could be seen in Figures 6 and 7. Figure 7a shows that the yellow region reflects the ST states. Its area/width represents the duty cycle of ST states. When the width changes, $\omega_m T_d$ varies, the harmonic amplitude H_{cm} in (13) and (18) varies. The integral of the harmonic amplitude in one modulation cycle would lead to the difference in the calculated total harmonic magnitude. The calculated harmonics magnitudes in one modulation cycle of two methods are very close to the simulation results in Table 4.

5 | EXPERIMENTAL RESULTS

Experiments were conducted to further verify the proposed theory and provide more accurate harmonics results. As shown in Figure 12, a 200 W single-phase Z-source inverter was built

and tested. The models of key power components are listed in Table 6. The controller is DSP28335. The diameter of the insulated copper wire in the two Z-source inductors is 0.5 mm to reduce the skin effect. Open-loop experiments were conducted and only the output voltage waveforms are presented in Figure 12 to compare output harmonics.

Detailed parameters of the circuit are listed in Table 5. The primary principle of designing these Z-source unit parameters C_{Z1}, C_{Z2}, L_{Z1} and L_{Z2} is to enable the storing and transferring of energy in order to boost output voltage and limit the voltage ripple. The desired capacitance of the Z-source capacitor could be determined as shown in (19), where α represents the ratio of capacitor voltage ripple by average capacitor voltage. D represents the duty ratio of shoot-through states, and f_s represents switching frequency.

$$C_{Z1} = C_{Z2} = \frac{i_C \cdot dt}{dV_C} = \frac{\overline{i_L} \cdot D}{\alpha \overline{V_C} f_s} \tag{19}$$

Similarly, the inductance of the Z-source inductor could be determined as shown in Equation (20) where β represents the

TABLE 5 Parameters of hardware experiments

Parameters	Values
Input DC voltage V_{in}	100 V
Rated V_{out} (peak)	200 V
Rated V_{out} (r.m.s.)	141 V
Switching frequency of carrier wave	10 kHz
Inductance of L_{Z1}, L_{Z2}	280 μH
Capacitance of C_{Z1}, C_{Z2}	2200 μF
Inductance of L_f	330 μH
Capacitance of C_f	80 μF
Load resistance per phase R_{load}	100 Ω
Rated output power P_{load}	200 W

ratio of inductor current by average inductor current.

$$L_{Z1} = L_{Z2} = \frac{v_L \cdot \mathrm{dt}}{dI_L} = \frac{\overline{V_C} \cdot D}{\beta \overline{I_L} f_s} \quad (20)$$

The parameters of the LC filter are determined by the desired cut off frequency to filter harmonics as shown in Equations (21) and (22) where R represents the equivalent load impedance.

$$L_f = \frac{R}{2\pi . f_c} \quad (21)$$

$$C_f = \frac{1}{2\pi . R f_c} \quad (22)$$

Figure 13 shows the input voltage V_{in} (light green) and output voltage V_{out} (blue) waveforms at rated steady operation state. A voltage probe is connected to the load resistor to show the output voltage waveform in the oscilloscope. The waveform of oscilloscope was then exported for post-analysis in MAT-LAB. The scope in Simulink replayed this waveform and calculated the THD value, then presented in Figure 14. The output voltage harmonics positively correlate with the shoot-through duty cycle when the control method of evenly-distributed ST states is adopted. For unevenly-distributed ST states, the THD varies when the duty cycle is small, while it positively correlates with the duty cycle when more ST states are inserted. This result matches the calculated conclusion and the simulations as described before. The overall THD is kept at a low-level lead by the output LC-filter, while the comparison of its harmonic feature remains.

6 | CONCLUSION

The mathematical relationship between the output harmonics and ST states with quantitative analysis for bipolar-modulation based Z-source inverters is described. A modified double-Fourier-transformation-based calculation scheme is proposed

(a)

(b)
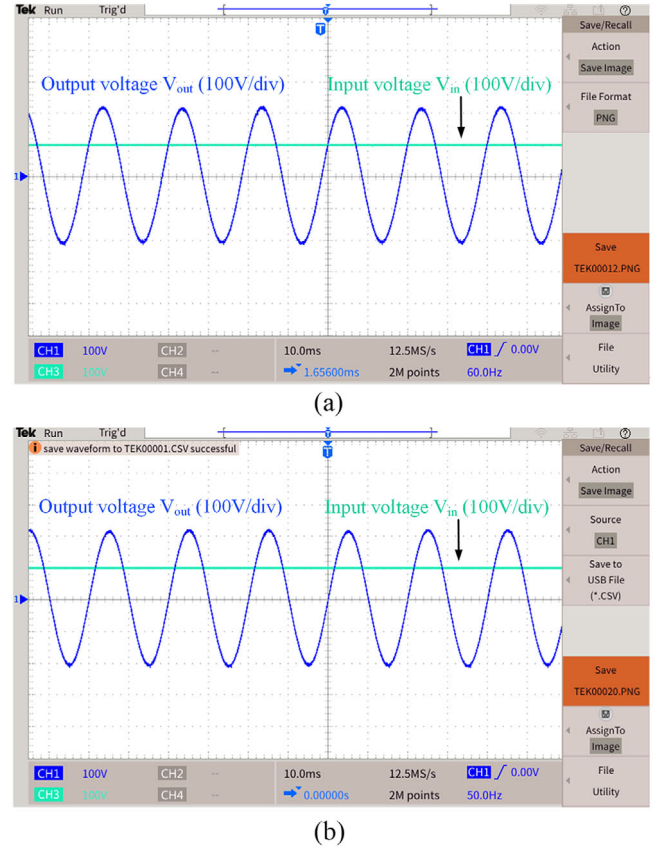
FIGURE 13 Output voltage waveform at rated output power (a) evenly-distributed method (b) unevenly-distributed method
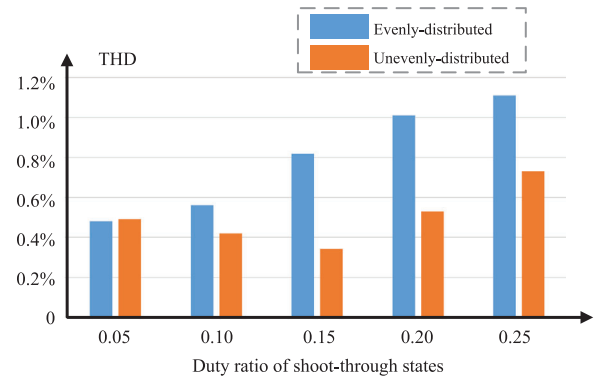
FIGURE 14 The THD of output voltage versus the ST states duty cycle (a) evenly-distributed method (b) unevenly distributed method

to estimate the output harmonics with different ST states insertion methods. It is verified by simulation and hardware experiments that the calculated harmonics magnitudes with ST states inserted match the experimental results well. For SPWM based single-phase Z-source inverters, the harmonics of unevenly distributed ST states mentioned in this paper is lower than that of the evenly distributed one. The proposed quantitative harmonics approach for single-phase Z-source inverters provides a helpful tool for design of bipolar-modulation based control methods in order to estimate and reduce the output harmonics.

ACKNOWLEDGEMENTS

CONFLICT OF INTEREST

The authors declare no conflict of interest.

DATA AVAILABILITY STATEMENT

Research data are not shared.

ORCID

Siu Wing Or https://orcid.org/0000-0003-2536-5658

REFERENCES

1. Bowes, S.R., Grewal, S.S.: Novel space-vector-based harmonic elimination inverter control. IEEE Trans. Ind. Appl. 36(2), 549–557 (2000)
2. Enjeti, P.N., Ziogas, P.D., Lindsay, J.F.: Programmed PWM techniques to eliminate harmonics: A critical evaluation. IEEE Trans. Ind. Appl. 26(2), 302–316 (1990)
3. Jiao, N., Wang, S., Liu, T., Wang, Y., Chen, Z.: Harmonic quantitative analysis for dead-time effects in SPWM inverters. IEEE Access 7, 43143–43152 (2019)
4. Chierchie, F., Paolini, E.E., Stefanazzi, L.: Dead-time distortion shaping. IEEE Trans. Power Electron. 34(1), 53–63 (2019)
5. Hwang, S., Kim, J.: Dead time compensation method for voltage-fed PWM inverter. IEEE Trans. Energy Convers. 25(1), 1–10 (2010)
6. Kumar, M.: Time-domain characterization of digitized PWM inverter with dead-time effect. IEEE Trans. Circuits Syst. I Regul. Pap. 65(10), 3592–3601 (2018)
7. Odavic, M., Sumner, M., Zanchetta, P., Clare, J.C.: A theoretical analysis of the harmonic content of PWM waveforms for multiple-frequency modulators. IEEE Trans. Power Electron. 25(1), 131–141 (2010)
8. Yang, Y., Zhou, K., Wang, H., Blaabjerg, F.: Analysis and mitigation of dead-time harmonics in the single-phase full-bridge PWM converter with repetitive controllers. IEEE Trans. Ind. Appl. 54(5), 5343–5354 (2018)
9. Cichowski, A., Nieznanski, J.: Self-tuning dead-time compensation method for voltage-source inverters. IEEE Power Electron. Lett. 3(2), 72–75 (2005)
10. Xu, W., Chan, K.W., Or, S.W., Ho, S.L., Liu, M.: A low-harmonic control method of bidirectional three-phase Z-source converters for vehicle-to-grid applications. IEEE Trans. Transp. Electrif. 6(2), 464–477 (2020)
11. Wu, C.M., Lau, W.-H., Chung, H.S.-H.: Analytical technique for calculating the output harmonics of an H-bridge inverter with dead time. IEEE Trans. Circuits Syst. I 46(5), 617–627 (1999)
12. Deng, H., Helle, L., Bo, Y., Larsen, K.B.: A general solution for theoretical harmonic components of carrier based PWM schemes. In: *2009 Twenty-Fourth Annual IEEE Applied Power Electronics Conference and Exposition*. Washington, DC, pp. 1698–1703 (2009)
13. Kostic, D.J., Avramovic, Z.Z., Ciric, N.T.: A new approach to theoretical analysis of harmonic content of PWM waveforms of single- and multiple-frequency modulators. IEEE Trans. Power Electron. 28(10), 4557–4567 (2013)
14. Noroozi, N., Zolghadri, M.R., Yaghoubi, M.: Comparison of common-mode voltage in three-phase quasi-Z-source inverters using different shoot-through implementation methods. In: *2018 IEEE 12th International Conference on Compatibility, Power Electronics and Power Engineering (CPE-POWERENG 2018)*. Doha, pp. 1–6 (2018)
15. Lei, Q., Cao, D., Peng, F.Z.: Novel loss and harmonic minimized vector modulation for a current-fed quasi-Z-source inverter in HEV motor drive application. IEEE Trans. Power Electron. 29(3), 1344–1357 (2014)
16. Pilehvar, M.S., Mardaneh, M.: Phase-shift control and harmonics elimination for H-bridge Z-source inverter. IET Power Electron. 8(4), 618–627 (2015)
17. Qi, Y., Fang, J., Liu, J., Tang, Y.: Coordinated control for harmonic mitigation of parallel voltage-source inverters. CES Trans. Electr. Mach. Syst. 2(3), 276–283 (2018)
18. Trinh, Q.N., Wang, P., Tang, Y., Choo, F.H.: Mitigation of DC and harmonic currents generated by voltage measurement errors and grid voltage distortions in transformerless grid-connected inverters. IEEE Trans. Energy Convers. 33(2), 801–813 (2018)
19. Arricibita, D., Sanchis, P., González, R., Marroyo, L.: Impedance emulation for voltage harmonic compensation in PWM stand-alone inverters. IEEE Trans. Energy Convers. 32(4), 1335–1344 (2017)
20. Sreekumar, P., Khadkikar, V.: Direct control of the inverter impedance to achieve controllable harmonic sharing in the islanded microgrid. IEEE Trans. Ind. Electron. 64(1), 827–837 (2017)
21. Itkonen, T., Luukko, J., Sankala, A., Laakkonen, T., Pollanen, R.: Modeling and analysis of the dead-time effects in parallel PWM twolevel three-phase voltage-source inverters. IEEE Trans. Power Electron. 24(11), 2446–2455 (2009)
22. Mirzaeva, G., Goodwin, G.: Harmonic suppression and delay compensation for inverters via variable horizon nonlinear model predictive control. Int. J. Control 88(7), 1400–1409 (2015)
23. Qiu, T., Wen, X., Zhao, F.: Adaptive-linear-neuron-based dead-time effects compensation scheme for PMSM drives. IEEE Trans. Power Electron. 31(3), 2530–2538 (2016)
24. Tang, Z., Akin, B.: Suppression of dead-time distortion through evised repetitive controller in PMSM drives. IEEE Trans. Energy Convers. 32(3), 918–930 (2017)
25. Micallef, A., Apap, M., Spiteri-Staines, C., Guerrero, J.M., Vasquez, J.C.: Reactive power sharing and voltage harmonic distortion compensation of droop controlled single phase islanded microgrids. IEEE Trans. Smart Grid 5(3), 1149–1158 (2014)
26. Sonkar, S.P., Lal, V.N., Singh, R.K.: Three-phase quasi-Z source inverters with regulated multiple AC outputs for microgrid applications and three-phase residential load. IET Power Electron. 13(11), 2222–2235 (2020)
27. Faistel, T.M.K., Guisso, R.A., Andrade, A.M.S.S.: Evaluation of cascaded voltage step-up cells applied to the quasi-Z-source DC-DC converter. IET Power Electron. 13(15), 3273–3282 (2020)
28. Wang, R., Zhao, J., Liu, Y.: A comprehensive investigation of four-switch three-phase voltage source inverter based on double fourier integral analysis. IEEE Trans. Power Electron. 26(10), 2774–2787 (2011)
29. Holmes, D.G., Mcgrath, B.P.: Opportunities for harmonic cancellation with carrier-based PWM for a two-level and multilevel cascaded inverters. IEEE Trans. Ind. Appl. 37(2), 574–582 (2001)